REPORT DOCUMENTATION PAGE

AFRL-SR-BL-TR-01-

0575

1. REPORT DATE (DD-MM-YYYY)	2. REPORT TYPE	3. DATES COVERED (From - To)
24-Sept-2001	Final	20Sept00 - 19June01

4. TITLE AND SUBTITLE	5a. CONTRACT NUMBER
Space-Ready Polymer Nanocomposites	F49620-00-C-0057

5b. GRANT NUMBER

5c. PROGRAM ELEMENT NUMBER
65502F

6. AUTHOR(S)	5d. PROJECT NUMBER
D. Gerald Glasgow, Choongyong Kwag, Elliot B. Kennel	STTR

5e. TASK NUMBER
TX

5f. WORK UNIT NUMBER

7. PERFORMING ORGANIZATION NAME(S) AND ADDRESS(ES)	8. PERFORMING ORGANIZATION REPORT NUMBER
Applied Sciences, Inc. 141 West Xenia Avenue P.O. Box 579 Cedarville, OH 45314	

9. SPONSORING / MONITORING AGENCY NAME(S) AND ADDRESS(ES)	10. SPONSOR/MONITOR'S ACRONYM(S)
AFOSR/PKC 801 North Randolph Street, Room 732 Arlington, VA 22203-1977	11. SPONSOR/MONITOR'S REPORT NUMBER(S)

12. DISTRIBUTION / AVAILABILITY STATEMENT

AIR FORCE OFFICE OF SCIENTIFIC RESEARCH (AFOSR)
NOTICE OF TRANSMITTAL DTIC. THIS TECHNICAL REPORT
HAS BEEN REVIEWED AND IS APPROVED FOR PUBLIC RELEASE
LAW AFR 190-12. DISTRIBUTION IS UNLIMITED.

13. SUPPLEMENTARY NOTES

14. ABSTRACT

In this project, polymer nanocomposites based upon carbon nanofibers (CNFs) were investigated for aerospace applications. These nanocomposite materials are likely to enhance or enable diverse military and civilian aerospace capabilities. These include significant improvements for materials with tailored coefficient of thermal expansion (CTE), radar signature reduction coatings, static charge mitigation, compliant electrical conductors (e.g., for solar cell contacts), and structural materials property enhancement. In addition, potential spin-offs to the automotive industry (CTE-matched body components) and electronics (CTE-matched composites, static charge mitigation, electromagnetic interference reduction) were identified.

20011126 068

15. SUBJECT TERMS
Polymer, Sunshade, Carbon, Nanocomposite, Thermal conductivity

16. SECURITY CLASSIFICATION OF:			17. LIMITATION OF ABSTRACT	18. NUMBER OF PAGES	19a. NAME OF RESPONSIBLE PERSON
a. REPORT	b. ABSTRACT	c. THIS PAGE	UL		Marty L. Rochon
Unclassified	Unclassified	Unclassified		42	19b. TELEPHONE NUMBER (include area code) 937/766-2020 ext. 126

Standard Form 298 (Rev. 8-98)
Prescribed by ANSI Std. Z39.18

TABLE OF CONTENTS

LIST OF FIGURES

LIST OF TABLES

I. EXECUTIVE SUMMARY

In this project, polymer nanocomposites based upon carbon nanofibers (CNFs) were investigated for aerospace applications. These nanocomposite materials are likely to enhance or enable diverse military and civilian aerospace capabilities. These include significant improvements for materials with tailored coefficient of thermal expansion (CTE), radar signature reduction coatings, static charge mitigation, compliant electrical conductors (e.g., for solar cell contacts), and structural materials property enhancement.

In addition, potential spin-offs to the automotive industry (CTE-matched body components) and electronics (CTE-matched composites, static charge mitigation, electromagnetic interference reduction) were identified.

Ternary nanocomposites were found to be promising for CTE reduction and structural property enhancement. For example, a combination of chopped fiberglass and nanofibers demonstrated excellent performance. The CTE of fiberglass reinforced polyester, as used in sheet molding compounds, is typically 32 ppm/°C. Inclusion of 5% carbon nanofibers reduced this value to 25 ppm/°C. Positive effects were also demonstrated using nanoclays in combination with nanofibers. One shortfall from expectations came in the CTE behavior of CNF reinforced Derakane. However, the underperformance can be entirely attributed to a error in curing unrelated to the CNF reinforcement. This system couldn't be retested in the Phase I timeframe, but the error presents no meaningful impediment to Phase II progress. The conclusion is that CTE matching to structural aluminum and titanium is achievable with several different polymer systems, such as polypropylene and cross-linked polyester. This would allow structural applications to benefit from reduced weight and manufacturing cost, both in aerospace as well as commercial applications (such as automotives). With additional work, very low or zero CTE polymer composites for enhanced structural stability during orbital sunlit/darkside transitions are feasible.

Mechanically, cross-linked polyester (CLPE) nanocomposites with combined fiberglass and nanofiber reinforcement performed well.

Electrically, property enhancement was successfully demonstrated for several polymer systems. Static Charge dissipation and compliant electrical connectors are enabled. Various systems are also feasible for reduced radar cross-section materials.

Overall, feasibility of using CNFs to improve the properties of space qualified polymers was clearly demonstrated. In Phase I, the feasibility was demonstrated in proxy systems which are cheaper and easier to handle than space qualified systems. Phase II efforts will initially focus on translating positive Phase I results into actual space-qualified polymer materials, and expanding the range of systems under study. Later in the Phase II program, prototype fabrication and demonstration will be carried out for a variety of candidate applications. The relevant DOD components requiring this suite of composite properties as well as General Motors Research Center will be included as evaluators in the Phase II effort.

II. BACKGROUND

2.1 Carbon Nanofiber Background

Many types of carbon nanostructures have been identified since the discovery of the C_{60} molecule (referred to as a "fullerene" or "buckyball") which led to the 1996 Nobel Prize for Robert F. Curl, Harold W. Kroto and Richard E. Smalley. These nanostructures are typically classified as follows:

a. A *single-walled nanotube* (SWNT) is a cylindrical structure consisting of a single layer of carbon atoms. The diameter is typically about 1.35 nm, and the length can be a micron or more.

b. A *multi-walled nanotube* (MWNT) contains two or more concentric atomic layers, the eight-layer tube being common.[1] MWNTs include structures up to 10 nm in diameter, and are characterized by distinctly quantum phenomena in their transport characteristics.

c. *Carbon nanofiber* (CNF) is the term used to describe a structure greater than 10 nm in diameter. Among the CNFs, two distinct morphologies have been noted. (See Figure 1.) The first is a continuation from MWNT's in which the CNF contains additional concentric layers of carbon, oriented parallel to the nanofiber axis. We refer to these as concentric wall (CW) CNFs. The second is made up of cones of carbon stacked one into the next. [2,3,4,5] We refer to these as angled wall (AW) CNFs. In the AWCNF, the surface of the nanofiber contains exposed plane edges, an important consideration for chemical bonding. (Note that the sp^2 bonds on the face of a graphitic lattice are essentially inert, and thus bonding to a polymer matrix requires edge sites in order to have something to bond to. Edge plane sites are typically not present in MWNTs or CWCNFs.)

The above terminology is not completely standard within the scientific community, and the terms MWNT and "carbon nanofiber" are sometimes used interchangeably. However, the above terminology will be used throughout this report.
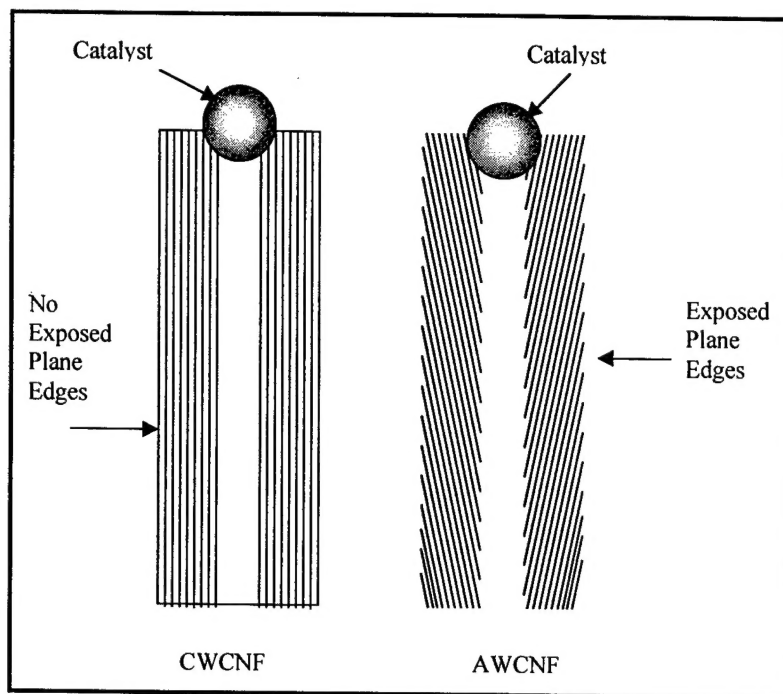
Figure 1. Comparison of the concentric and angled wall structures for CNFs.

Many studies have expanded the understanding of the formation and growth of nanofibers.[6,7,8,9,10,11,12,13] By keeping the nanofibers in the production furnace longer, a chemical vapor deposition (CVD) carbon overcoat is produced. Conversely, when the residence time is shortened, the CVD overcoat can be avoided. This is shown in Figures 2 and 3.
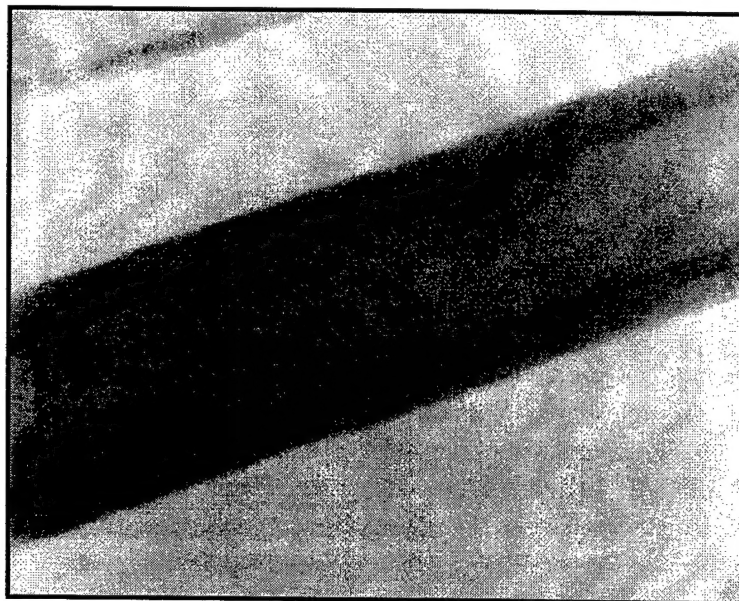
Figure 2. Transmission electron micrograph (TEM) of Pyrograf®-III CNF. The highly-ordered, catalytically grown carbon (dark and light banded structure on either side of hollow tube center) is surrounded by a CVD layer of turbostratic carbon (medium gray).
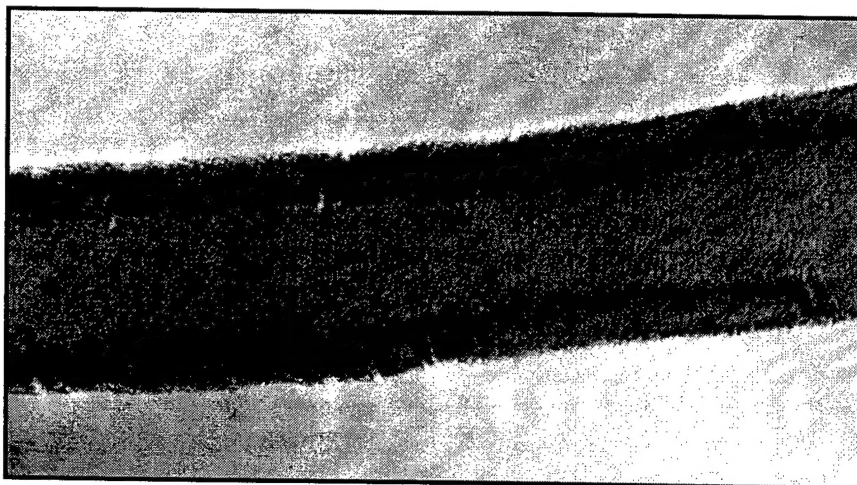
Figure 3. CNF with no visible CVD layer.

When graphitized, the overcoat may provide additional structural integrity as well as electrical conductivity.   Other applications may be better served without a CVD overcoat, since good bonding can be expected to exposed edge plane bonding sites. In most cases, heat treatment can be avoided.

Carbon nanofibers, designated as Pyrograf®-III,   are produced by Applied Sciences, Inc. (ASI). These nanofibers can ultimately be very economical since they are grown using inexpensive coal or natural gas as a feed material, and because the fiber is produced in a simple, one-stage process.[14] In many respects the process is similar to that used for producing carbon black.

Figure 4 illustrates the production system used for to make the CNFs for this project.   Gas phase reactants are introduced into a heated furnace, where the decomposition of the gaseous compounds generate the species required for nucleation and growth of nanoscale carbon fibers with highly graphitic structure.
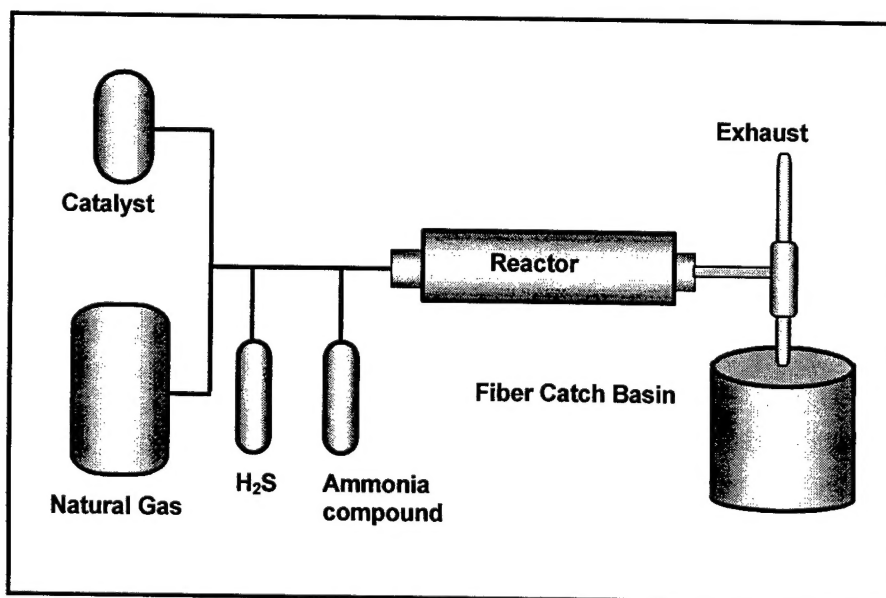
Figure 4. Schematic of the CNF synthesis reactor system.

2.2 Goals for Polymer Nanocomposites

Polymer nanocomposites can now be inexpensively manufactured, providing a low-cost method to attain high performance materials for space use. Particularly for low-earth orbit, such materials offer the potential for excellent resistance to threats such as thermal distortion during transition from earth shadow to sunlit conditions; atomic oxygen; debris; proton flare and others. In addition, such materials can mitigate static charge buildup and offer reduced radar cross section, due to high absorption in optical and radar bands. In many cases, performance comparable to carbon-epoxy composites can be obtained. Yet, unlike cloth-reinforced polymers, the nanocomposite polymer can be used for inexpensive manufacturing processes such as transfer molding, injection molding and so on.

Here follows a list of the important properties desired from polymer nanocomposites and discussion of the impact of CNFs in attaining these properties.

a. *Engineered coefficient of thermal expansion (CTE)*, resulting in highly stable components which can tolerate sunlit/earth shadow transitions without expansion and contraction. Such behavior is important for very quiescent platforms, such as space surveillance and reconnaissance platforms, which need to avoid vibration. Modification of CTE with CNFs is possible because the slightly negative CTE of the CNFs can be used to offset the positive CTE of a polymer. By appropriate combination of the CNFs and polymer matrix it is possible to develop nanocomposites with reduced or even zero CTE. Note also that the CTE of a composite is weighted more heavily by the material with the higher modulus. Since the modulus of the CNFs is many times greater than the polymer matrix, CTE control can be achieved with relatively low loadings of nanoifbers.

Note also that electronic components, such as chip modules, must match the CTE of the semiconductor materials (silicon or gallium arsenide) in the chip to the carrying/cooling substrate on which the chip is mounted. Thus engineered CTE can be a significant asset for aerospace electronic designs.

ASI, along with General Motors R&D Center, has demonstrated this effect in the polypropylene system.[15] Briefly, the data shows that 15 vol % CNF reduces the CTE from 200 ppm/°C to about 50 ppm/°C at 100 °C. Note however, that polypropylene is not the best candidate for highly stable spacecraft. A material such as Kapton, having a low CTE to begin with, as well as excellent mechanical properties, outgasing characteristics, threat resistance, etc., is likely to be much better.

CTE, ppm/°C
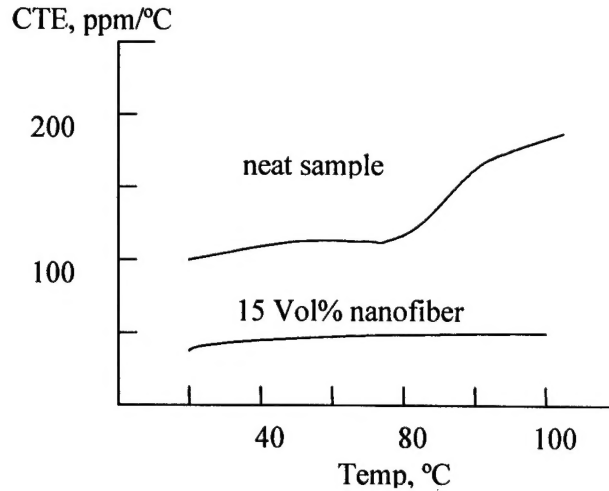
Figure 5. CTE of polypropylene samples with and without CNF addition. Similar effects are expected for other polymer nanocomposites.

b. *Improved strength and modulus.* Nanocomposites can have significantly improved strength and modulus compared to the neat material. Accordingly, lighter weight and reduced resonance during launch vibration is possible for components manufactured from polymer nanocomposites. The modulus of a fiber reinforced composite can be predicted by Cox's theory.[16] The modulus of the composite depends upon the fiber volume fraction V_f, the fiber and matrix moduli E_f and E_m, respectively, the length to diameter ratio of the fiber through a function $g(l/d)$, and the degree of orientation through a function $f(\theta)$:

$$E = E_m (1-V_f) + E_f V_f f(\theta) g(l/d) .$$

For isotropic 3-D orientation $f(\theta) = 1/6$, for random orientation in 2-D $f(\theta) = 1/3$, for perfect 1-D alignment $f(\theta) = 1$. For carbon fibers with $l/d > 100$, $g(l/d)<1$.

Just as with continuous fiber-reinforced composites, there are structural benefits of anisotropy in short fiber composites. For example, sheet molding compound (SMC) which has glass fibers roughly aligned in 2-D, makes stiffer panels than a composite with equivalent volume fraction of fibers oriented in 3-D. If the Pyrograf-III fibers can be grown to an $l/d \gg 100$, and oriented in two dimensions, the Cox theory predicts that the composite will be up to nine times as stiff as the glass-reinforced SMC. With only 30% volume fraction of fiber, the panel would exhibit equivalent stiffness to aluminum.

Discontinuous fiber has also been used to enhance the strength of material in several composite systems[17,18,19] Composites with ordered whiskers exhibited higher strength and modulus. Good adhesion between these carbon nanofibers and matrix resins is essential for the performance of any composite material, so the mechanical properties of composites are strongly influenced by fiber surface morphology and chemistry.[20] Two key parameters influencing adhesion are fiber surface area and energy

10
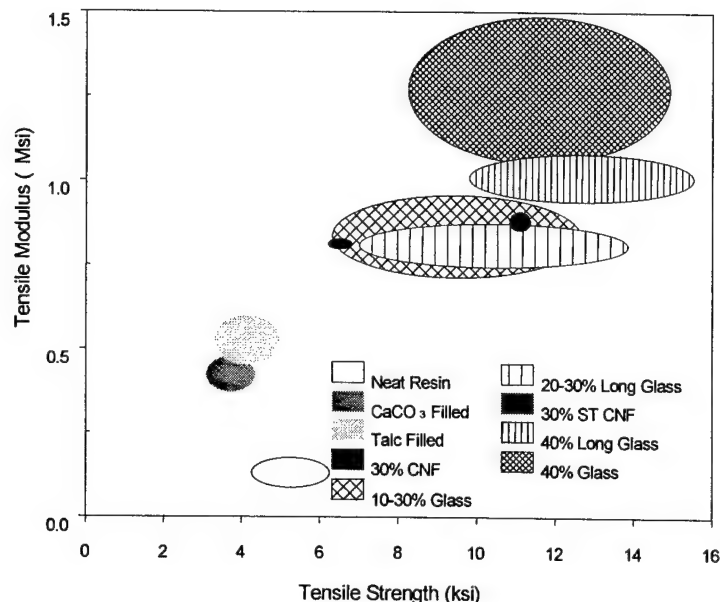
Figure 6. Ranges of modulus and strength for different types of reinforcement in polypropylene. Recent improvement in CNF nanocomposite strength and modulus have been achieved various surface treatments (ST) to improve the quality of the CNF/matrix interface. (Compare CNF and ST CNF points in the figure.)

The tensile strength of a fiber-reinforced composite is a reflection of the adhesive forces between the fiber and matrix resin. Tensile strength increases as the strength of the interfacial bond increases and the strength of this bond is strongly influenced by the wettability of the fiber by the matrix resin. Fiber wettability is, in turn, related to the surface energy of the fiber and the available surface area.

Fibers with differing surface characteristics were produced by using various exposures to oxidizing agents such as air. The surface energies and surface areas were measured, and then the samples were used to prepare polypropylene composites containing 15 vol.% nanofibers which then were used for determination of tensile strength and modulus. The tensile strengths obtained for composites containing fibers with widely ranging surface energies show the influence of the fiber interfacial properties. This effect can be seen more clearly when the tensile strengths are plotted vs external surface area and adjusted surface energy as shown in the contour plot shown below. Although this data applies to polypropylene, the same methodology is applicable to generic composite systems. It shows that mechanical properties of such materials are clearly enhanced by carbon nanofibers, and can be optimized through a rigorous process.
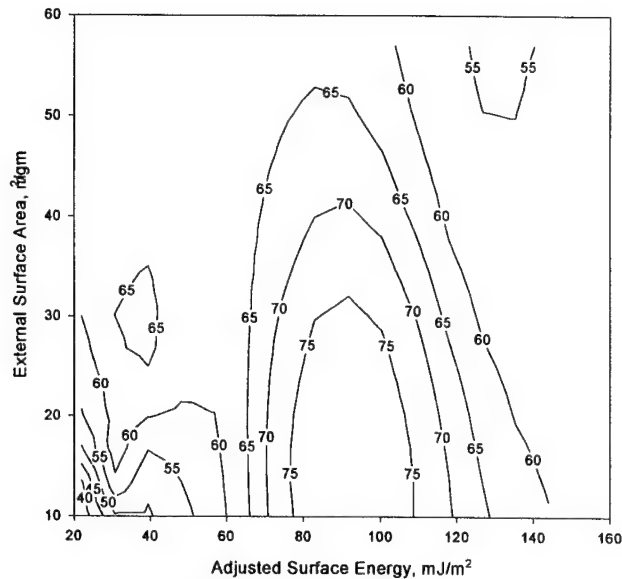
Figure 7. Contour Plot of Tensile Strength (MPa) vs Surface Area and Surface Energy.

      c. ***Improved static charge dissipation.*** Static charge dissipation and system generated electromagnetic pulse (SGEMP) effects result when static charge builds up at a high voltage on a dielectric surface. This is a serious problem for many spacecraft. Conductive polymer nanocomposites would eliminate such problems. As shown below, the addition of the nanofibers reaches a percolation threshold at only a few volume percent reinforcement.
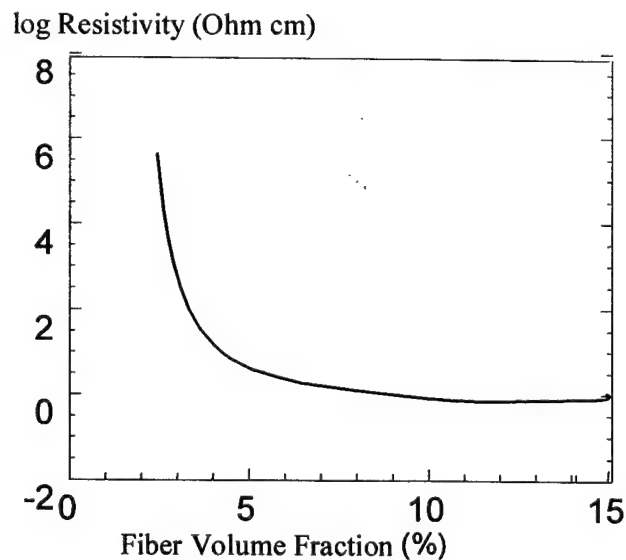
Figure 8. Electrical resistivity in polypropylene.

      d. ***Low observability.*** The carbon nanofibers, because of their small size and electromagnetically "lossy" character, result in excellent absorption of radar. In addition

to being of high interest for aircraft and other terrestrial military assets, reduced radar cross section can be an advantage for satellites as well, making it more difficult for potential adversaries to observe US space-based assets or to obtain tactical sensor information (i.e., radar lock-on).

Nanocomposites can be a nearly ideal receptor for radar waves, making them useful for low observable applications. Theory indicates that long, small-diameter filaments with moderate electrical conductivity lead to the best radar extinction efficiency (i.e., cross section per unit volume or mass of material).[21,22,23] ASI has previously fabricated thin coatings that incorporated carbon nanofibers into silicone. These coatings were characterized at Lockheed-Martin Tactical Aircraft Systems in the frequency range from 2-18 GHz. The work is described in greater detail elsewhere in this report. The effort indicated dielectric constants that compare favorably with other state-of-the-art materials used in the low observable field.

e. ***Improved thermal conductivity***. Perhaps the most remarkable property of highly ordered graphite is its extraordinary thermal conductivity. The intrinsic conductivity of the nanofibers is placed at 1950 W/m-K, just below that of single crystal graphite and diamond, and far superior to the best competing carbon fiber, K-1100, which has a nominal conductivity of 1100 W/m-K. However, effects of the interface region between nanofiber and matrix, which is not accounted for by rule-of-mixtures approaches, likely dominate the nanocomposite conductivity so that there is very little enhancement in thermal conductivity from a true nanofiber.

Accordingly, high thermal conductivity composites can be better fabricated using a reinforcement material with less surface area per unit volume. Such a material can be created by varying the normal nanofiber growth protocol to permit a thicker layer of pyrolytic graphite to be deposited, such that the diameter can be increased to the micron level or more, resulting in a "microfiber," which ASI has recently produced (initially, as a battery electrode material) under the trade name Pyrograf®-IV. High thermal conductivity can be produced by graphitizing these "microfibers" at 3000 °C to produce a fiber thermal conductivity of 1950 W/mK. This step adds to the cost of the material, but is not technically challenging.

The composite thermal conductivity of a composite with finite-length reinforcement is given by

$$k_{comp} = k_{matrix}\left(1 - V_f\right) + F_1(\theta)F_2\left(\frac{L}{D}\right)F_3\left(\frac{A}{V_{fiber}}\right)k_{fiber}V_f \ ,$$

where k_{comp} is the thermal conductivity of the composite; k_{matrix} is the thermal conductivity of the matrix only; V_f is the fiber reinforcement volume fraction; $F_1(\theta)$ is a correction factor for the orientation of the fiber reinforcement = 1/3 for random orientation; F_2 is the correction factor for the finite length of the reinforcement = $2(L/d)\sqrt{\tanh(2L/d)}$; and k_{fiber} is the fiber reinforcement thermal conductivity = 1950 W/m-K. The remaining correction factor F_3 has been measured empirically at .71 for

Pyrograf®-I, and .0108 for Pyrograf®-III. A log-log interpolation yields an estimate of about 60 W/mK for a 50% nanofiber silicone nanocomposite for Pyrograf®-IV.

Table 1. Summary of Pyrograf® nanocomposite
options for thermal conductivity in polymeric materials.

Material	Diameter, microns	Length, microns	Surface Area to Volume Ratio, m^{-1}	Polymer composite thermal conductivity, W/m-K
Pyrograf®-I	10	30,000	4×10^5	up to 661
Pyrograf®-III	.05-0.20	100	2×10^7	1-10
Pyrograf®-IV	1	100	4×10^6	never measured; >60 expected.

f. *Compatibility with spacecraft environmental effects*. Carbon is a low-z, high temperature material and thus is one of the best possible materials for complying with x-ray threat scenarios. Similarly a nanocomposite is expected to have excellent resistance against natural radiation threats such as solar protons and cosmic rays. The 3-D reinforcement inherent to nanocomposites mitigates micrometeoroid threats. Polymer matrix composites are used in the fabrication of external and interior components of spacecraft placed in low earth orbit. Currently, fiber-reinforced-composite face sheets are frequently used in combination with aluminum honeycomb to form the external structure of the craft. The fiber-reinforced-composite/aluminum honeycomb sandwich provides good performance in terms of high strength, low weight, and low thermal distortion. This external structure also protects interior components and elements of the spacecraft from damage produced by the hypervelocity impact of small micrometeoroids and fragments of orbital debris. Hypervelocity impact tests of various composite materials normally produce varying levels of delamination in the material surrounding the damage site. In addition, a portion of the delaminated material can separate from the spacecraft, becoming fragments of orbital debris that pose a threat to other spacecraft. Use of a nanocomposite polymer as the face sheet of a honeycomb sandwich or other structural element of the spacecraft should minimize or eliminate delamination of the composite as a damage mechanism.

g. *Affordability*. The processes developed by ASI for producing carbon nanofiber additives is a revolutionary one, resulting in continuous, low cost fabrication of nanofibers used as the reinforcement in the polymer nanocomposite systems. Although the arguments concerning the properties of nanocomposites and the ability to integrate these materials to spacecraft are persuasive, the most important parameter is still *cost*. A revolutionary improvement in the production cost has been achieved by the development of a continuous process for producing carbon nanofibers referred to as Pyrograf-III. In this process, the organometallic catalyst and natural gas are introduced into one end of a tubular reactor and fibers are blown out the other end. This process has facilitated increased efficiency due to higher production rates and the elimination of furnace cool-down and the use of inert gas. Further economic improvements which can be gained in

manufacturing scale-up include use of inexpensive natural gas as a hydrocarbon feedstock, and more complete utilization of the remaining fuel and energy following the Pyrograf-III reaction. Very exotic types of nanomaterials, such as single walled nanotubes, are currently priced at hundreds of thousands of dollars pound, and thus are not affordable for most real-world applications. Currently, carbon nanofibers are sold at tens of dollars per pound

III. EXPERIMENTAL

Several composites based on thermoset resins, polyurethanes and thermoplastics were fabricated, including ternary composites including cross-linked polyester-fiberglass, cross-linked-polyester/silica, Noryl-, nylon, silicone, and others.

CTE measurements were made using two different methods. A laser dilatometer was used at the University of Dayton Research Institute. A mechanical dilatometer was used at General Motors Research.

While polyester resins have been used throughout commercial markets for many years, the need for improved thermal and mechanical properties for use in various environments has led to increased use of vinyl-ester resins.

A commercially available resin for use in composite fabrication is Derakane 470-45, having a 55% vinyl-ester and 45% styrene composition by weight. As shown in Figure 9(a), the vinyl-ester monomer coupled with the styrene monomer has reactive sites available for both free radical copolymerization and ionic copolymerization, depending on the initiator used. If a combination of initiators is used for catalysis, the resultant thermosetting copolymer forms a complex structure having a variety of possible branching and crosslinking variations.[24] Benzoyl peroxide, whose structure is shown in Figure 9(b), is a commonly used initiator because it readily decays into two like radicals under small amounts of heat. N,N-dimethylaniline can be used as an initiator in anionic copolymerization due to the nucleophilic nitrogen atom, see Figure 9(c).
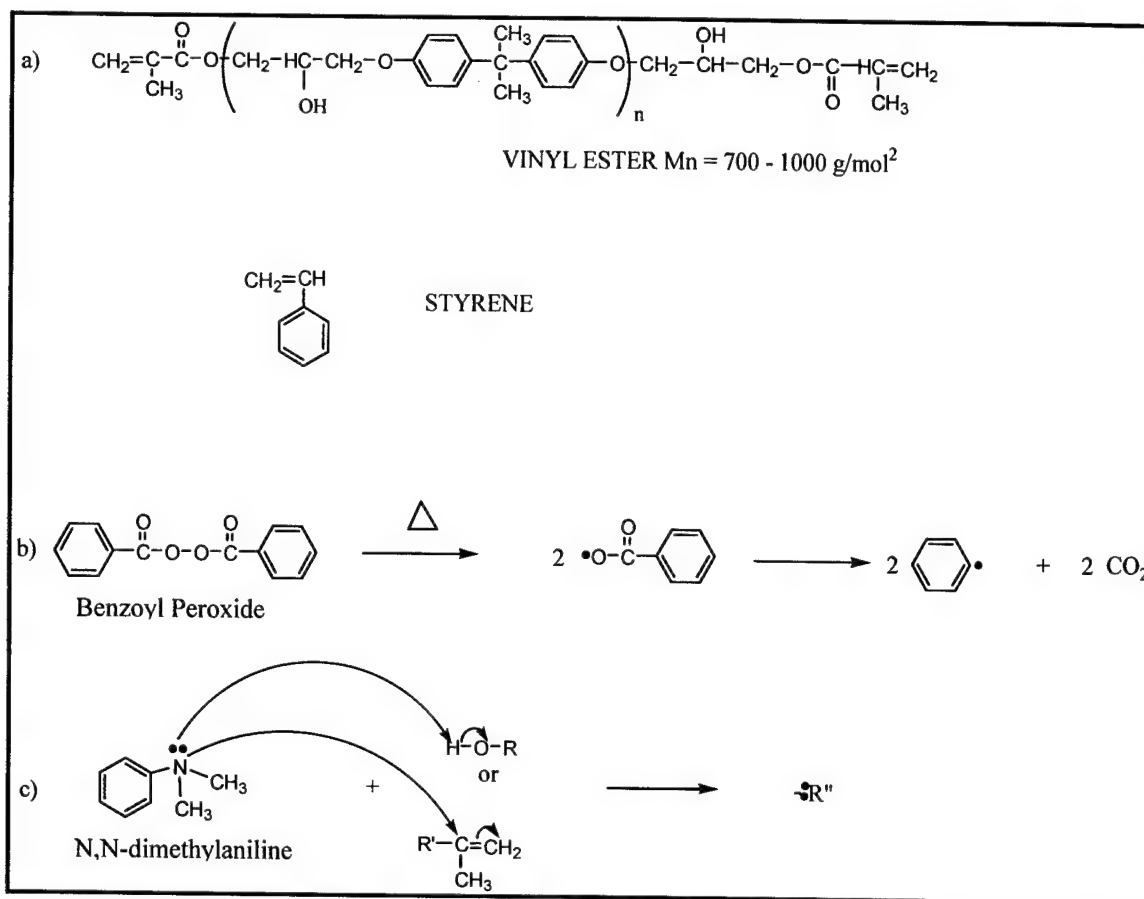
Figure 9. (a) Chemical structure of vinyl-ester—styrene resin found in commercial blends. (b) Chemical structure of benzoyl peroxide and its decay with heat. (c) Chemical structure of N,N-DMA and its predicted reactions with the hydroxyl or allyl groups of vinyl-ester. (See Figure 11, sites *a* and *b*.)

When benzoyl peroxide is used as a free radical initiator for copolymerization, the three-step initiation, propagation, termination reaction of free radicals will result in a variety of products. Figure 10 shows the first step in the formation of polystyrene using a benzene radical as the initiator.
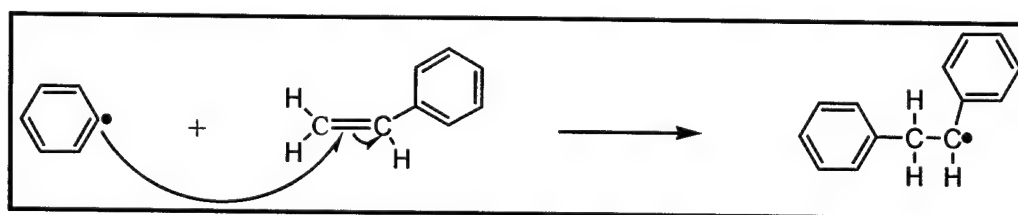
Figure 10. Benzene radical reaction with styrene double bond. A similar reaction occurs with the end-molecules of the vinyl-ester monomer. (See Figure 11, site *a*.) [4].

When N,N-dimethylaniline is used to initiate an anionic copolymerization cure process, the reaction begins as seen in Figure 9(c). Figure 11 shows the reactive sites of the vinyl-ester monomer attacked by a free-radical or ionic initiator. It is favorable for a styrene radical or ion to attack at these sites because they are relatively unshielded.
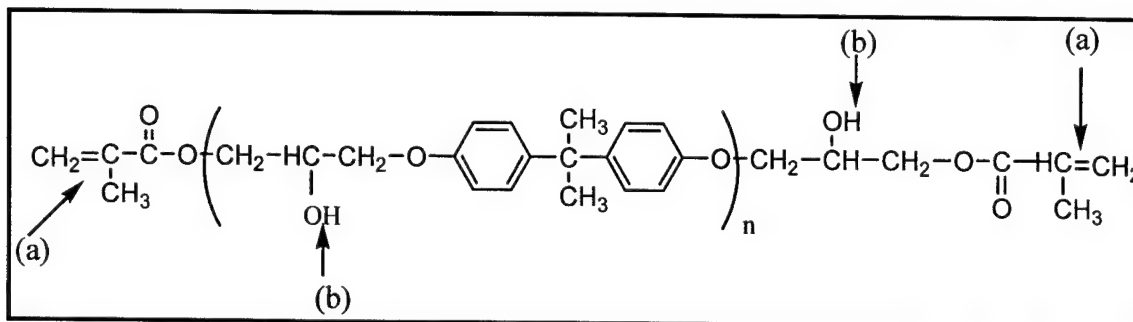
Figure 11. Chemical structure of vinyl ester showing reactive sites.

A schematic representation of the free-radical-initiated and the anionic-initiated copolymer reactions are shown in Figures 12 and 13 respectively.
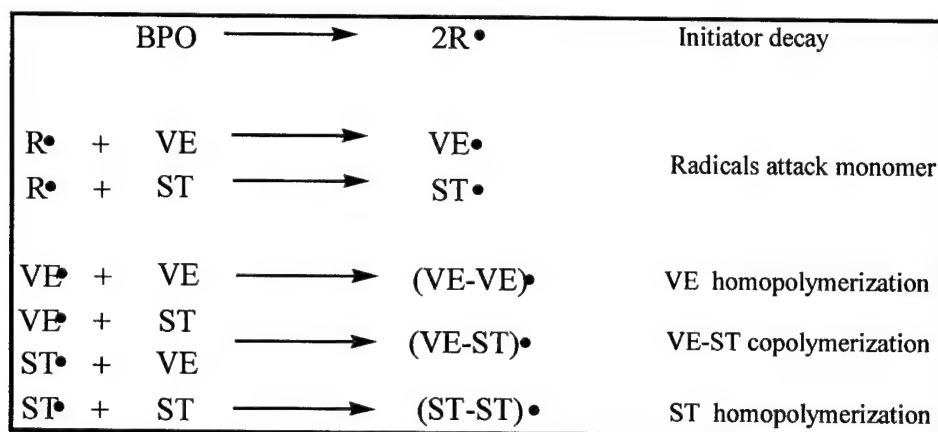
Figure 12. Free-radical initiated copolymerization where BPO = benzoyl peroxide, VE = vinyl ester, and ST = styrene. Polymerization continues to propagate until the reaction of one radical with another.

| (a) DMA | + | C≡C | ⟶ | DMA—C-C: |
| (b) DMA | + | H-O-R | ⟶ | DMA-H + :O-R |

C-C:	+	VE	⟶	VE-VE:	-or-	ST-ST:
:O-R	+	ST	⟶	VE-ST:		
C-C:	+	ST	⟶	VE-ST:	-or-	ST-ST:
:O-R	+	VE	⟶	VE-VE:		
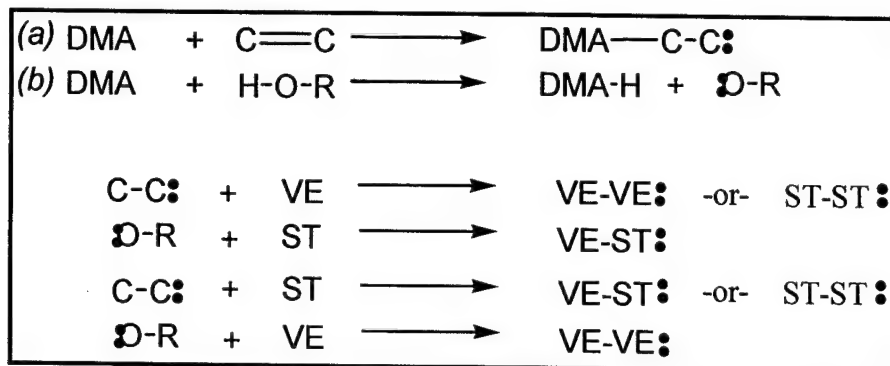
Figure 13. Schematic representation of anionic copolymerization and homopolymerization where (a) correlates with both the reaction at site (a) indicated in or the reaction between DMA and styrene . (b) indicates a reaction between DMA and vinyl-ester monomer at site (b).

When a combination of both free-radical and anionic initiators is used, a complex copolymer network containing a combination of their respective products will result. The preceding reactions also result in branching and crosslinking due to the many available reactive sites on the vinyl-ester monomer.

The extent of copolymer reaction and matrix crosslinking is strongly dependent on cure temperature. Differential scanning calorimetry (DSC) can be used to observe the progress of the reaction of a vinyl-ester—styrene resin as it is heated. The results of DSC analysis of the uncured mixture of polymer components will reveal an approximate range of the cure exotherm and will reveal the temperatures where the styrene and vinyl-ester monomers polymerize.

DSC analysis can be complemented by dynamic mechanical analysis (DMA) in which a sinusoidal strain is applied to a small, rectangular sample of copolymer. Because of its viscoelastic effects, the resulting stress will have a phase shift which varies as a function of temperature. This phase shift is described by the variable δ.[25] The DMA results can be analyzed in terms of the storage modulus and loss modulus:

$$\text{Storage modulus} \qquad E' = \left(\frac{\sigma^\circ}{\varepsilon^\circ} \right) \cos \delta \qquad\qquad (1)$$

$$\text{Loss modulus} \qquad E'' = \left(\frac{\sigma^\circ}{\varepsilon^\circ} \right) \sin \delta \qquad\qquad (2)$$

$$\tan \delta = \frac{E''}{E'} \qquad\qquad (3)$$

Where ε° is the amplitude of the applied strain, σ° is the amplitude of the stress response, and δ is the phase angle between the stress and the strain. A plot of the tan δ as a function of temperature will result in a peak in the range of the T_g. Thus, DMA can

reveal important information about the mechanical properties of storage modulus and T_g of a polymer.

Thermal Mechanical Analysis (TMA) is the method we used for characterizing the linear thermal expansion behavior of the composites. The TMA method involves using a precision probe that rests against the surface of a sample and is coupled to an LVDT detector. The sample resides in a heated chamber. Changes in height of the probe as the sample is heated reflect the thermal expansion of the sample.

Sample Preparation / Processing

Composite plaques were fabricated using the following materials and mixture ratios shown in Table 2.

Table 2. Composition of plaques.

Plaque	Material	Content (parts by weight)
C00	Derakane 470-45	100
	Silica, PPG ABS	47
	Benzoyl Peroxide	1.5
	N,N-Dimethylaniline	0.1
	Pyrograf III^{TM} (CNF)	0
C15	Derakane 470-45	100
	Silica, PPG ABS	47
	Benzoyl Peroxide	1.5
	N,N-Dimethylaniline	0.1
	Pyrograf III^{TM} (CNF)	1.5
C30	Derakane 470-45	100
	Silica, PPG ABS	47
	Benzoyl Peroxide	1.5
	N,N-Dimethylaniline	0.1
	Pyrograf III^{TM} (CNF)	3.0

Fifty grams of Derakane 470-45 vinyl-ester resin were used as a basis for formulation. The amount of material needed for each plaque and the size of the mixing device used were considered in determining this basis. Derakane 470-45 is a product of Dow Chemical Company (Freeport, TX) and contains a 55/45 ratio of vinyl-ester and styrene monomers, respectively. All materials were weighed in a fume hood and placed in covered glass jars for transport to a 3" diameter roll mill; however, because of the high toxicity of N,N-dimethylaniline (N,N-DMA), a 10 mL syringe was used to prepare and inject the N,N-DMA into the mixture. To increase the viscosity of Derakane 470-45 so that a roll mill could be used for mixing, approximately 50% of the total weight of silica was added and stirred into the total amount of Derakane 470-45 prior to mixing on the roll mill. It was found that additional silica could not be mixed in by hand.

The Derakane 470-45/silica mixture was then poured out onto a lab scale, 2-roll mill, having two 3" diameter rolls, and mixed. After adequate mixing of the initial

charge, 25% of the total silica was added onto the roll mill. Following several minutes of mixing, the catalysts, benzoyl peroxide (BPO) and N,N-DMA, were added simultaneously immediately followed by the addition of the final 25 pbw silica and the appropriate amount of Pyrograf®-III CNF (0%, 1.5%, or 3.0%). The mixture became rather friable and required that a pan be used to catch clumps of material falling off the mill rolls. This material was immediately put back onto the mill for mixing. After an additional 3-6 minutes of mixing, the material became soft in texture and held together in a uniform, smooth sheet. At this stage it was found that the material would cling so as to form on only one of the two rolls. If the material were left on the roll mills for more than 4-5 minutes after the initial change to a smooth material texture, it would again become friable and flake off of the roll mill. As a result, it was essential that the material be removed from the roll mill and placed into a mold during the stage in which the mixture was soft and pliable and uniformly held together.

A stainless steel mold was used to prepare samples having dimensions of 4.5" x 1.25" x 0.25" (length x width x height). The material was removed from the roll mill in one continuous, smooth sheet. Two edges were placed in the mold and the remaining two edges cut from the raw sheet with a knife. The mold was covered with a thin sheet of stainless steel and placed in a PHI press (1966-Pasadena Hydraulics Inc., El Monte, California) having a 4" ram and a 1.6 KW, 6.8 amp heater. The mold was subjected to 10,000 lbs ram force at room temperature for 15 minutes. The press was then heated, isobarically, from room temperature to a set-point temperature of 300°F (148.9°C), which is in the middle of the range of the cure exotherm. The temperature ramp for the PHI press was recorded using a Type K thermocouple and is seen in Figure 14. It was found that the press heating element had a ramp of 11.3 °F/min (4.5 °C/min) and an offset of minus 1°C from the set point. The mold containing the composite plaque was cured for 60 minutes (15 minutes at RT, 30 minutes undergoing a temperature ramp, and 15 minutes at a constant temperature of 149°C). The time used for curing was based on a gel-time of 50-70 minutes, approximated by observing when the composite hardened to its final, brittle physical state at ambient temperature and pressure.
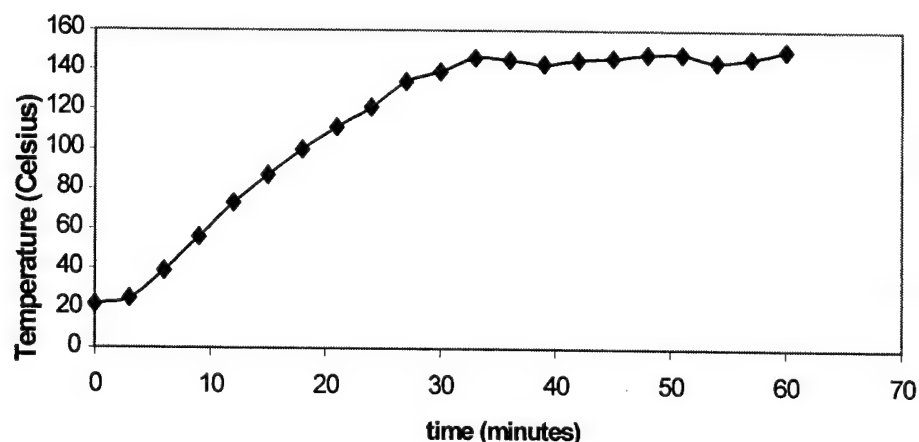
Figure 14. Temperature profile for press used to cure composite plaques.

The plaques were allowed to cool to room temperature for 2 hours or more before being removed from the mold. It was found that plaques having 0% carbon nanofiber had a density of 1.21 g/mL, those having 1.5% had a density of 1.23 g/mL, and those having 3.0% had a density of 1.26 g/mL. Additional, less-satisfactory, curing methods that were investigated are listed in Appendix A.

IV. RESULTS

4.1 Electrical Resistivity

Electrical resistivity in a nanocomposite is a function of the respective conductivities of the nano-reinforcement as well as the matrix material. In addition, the interaction layer between matrix and nano-reinforcement is also important, though difficult to evaluate.

The intrinsic conductivity of several different nanofibers was measured by compressing a pill of nanofibers-only (i.e., nanofibers in air, with no matrix material). The PR-xx designation refers to the gas protocol used for nanofibers, including gas composition, residence time and furnace temperature. PR-24 contains very little CVD layer on the surface, and thus has a small diameter (~50 nm). PR-19 consists of a catalytic core and CVD surface layer. The overall diameter is about ~180-200 nm.

The designation AG refers to as-grown material, with no surface treatment. PS means pyrolytically stripped material, with the surface devolitalized by heat. HT means heat treated material at 3100 C to achieve full graphitization.
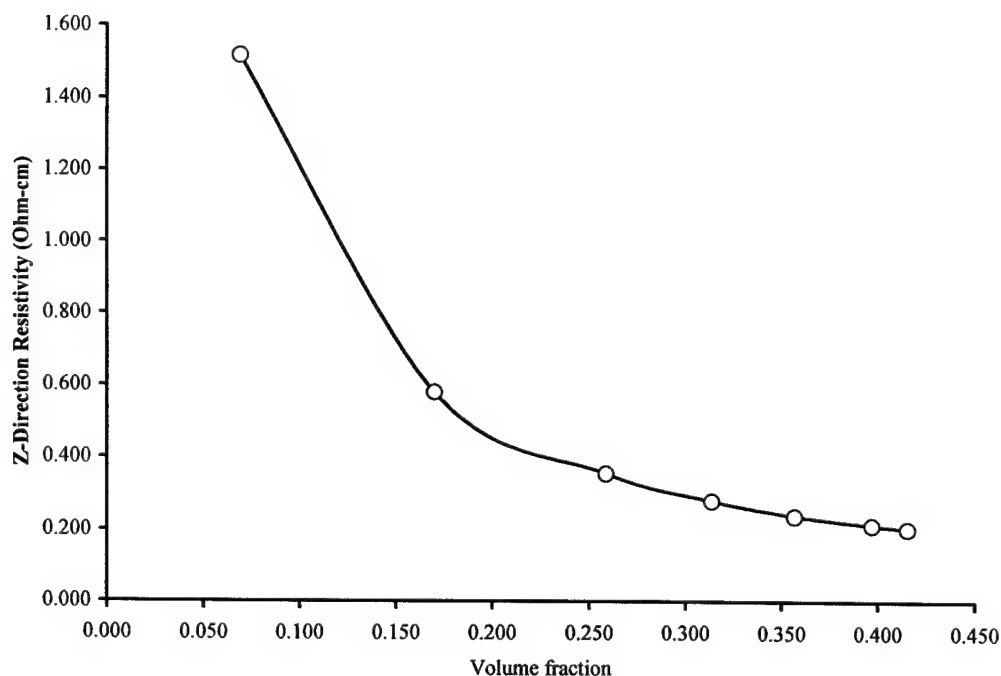
Figure 15. Z-Direction resistivity for PR-19-AG.
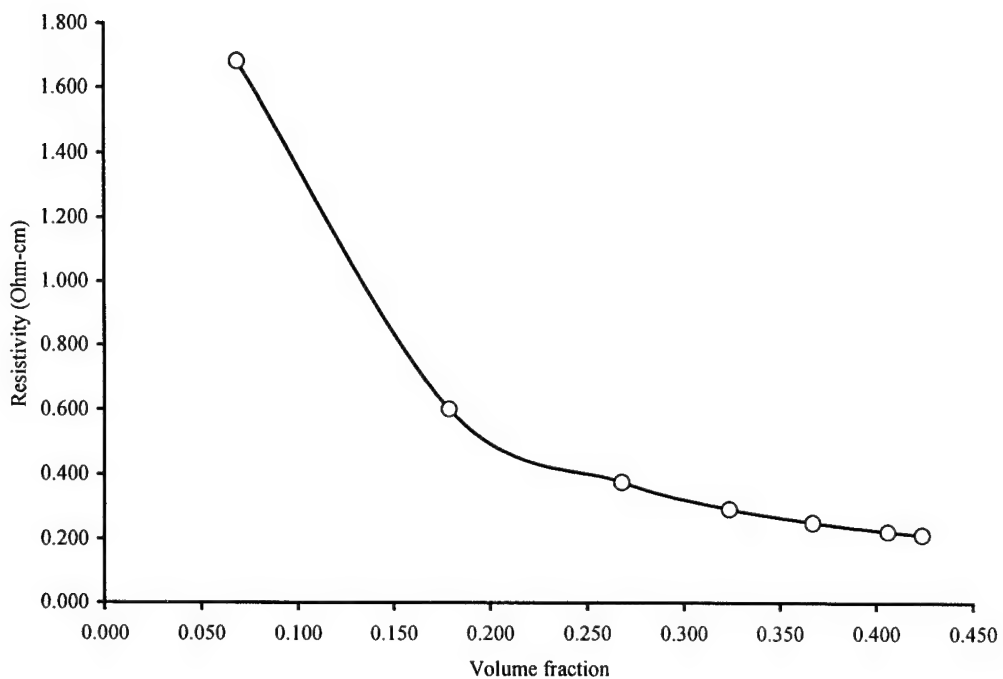
Figure 16. Z-Direction Resistivity for PR-24-AG.
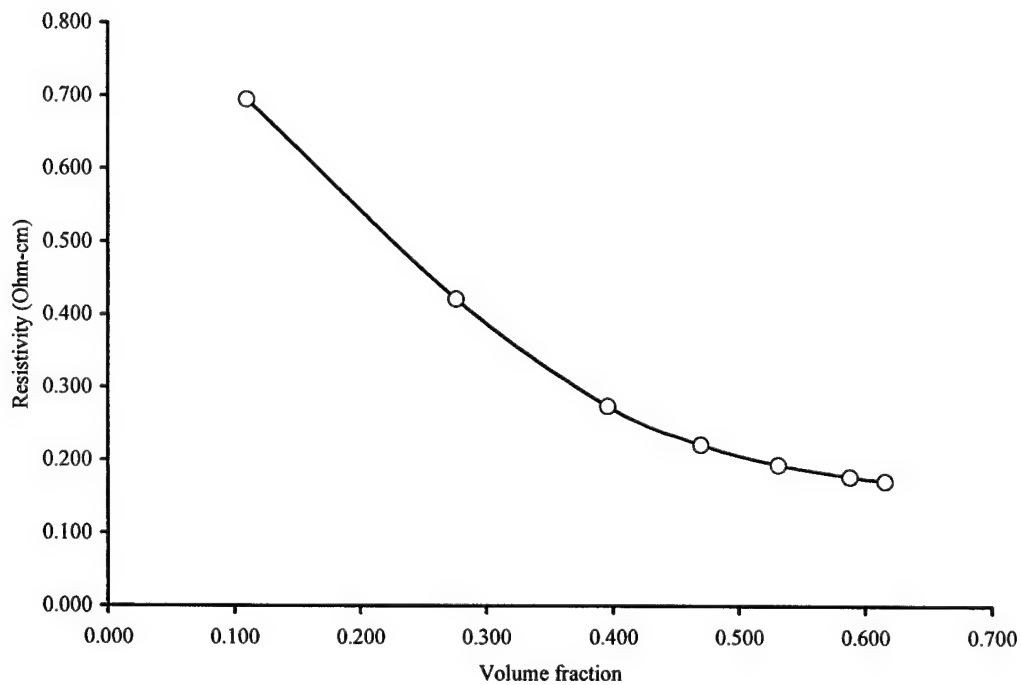
Figure 17. Z-Direction Resistivity for PR-19-HT.
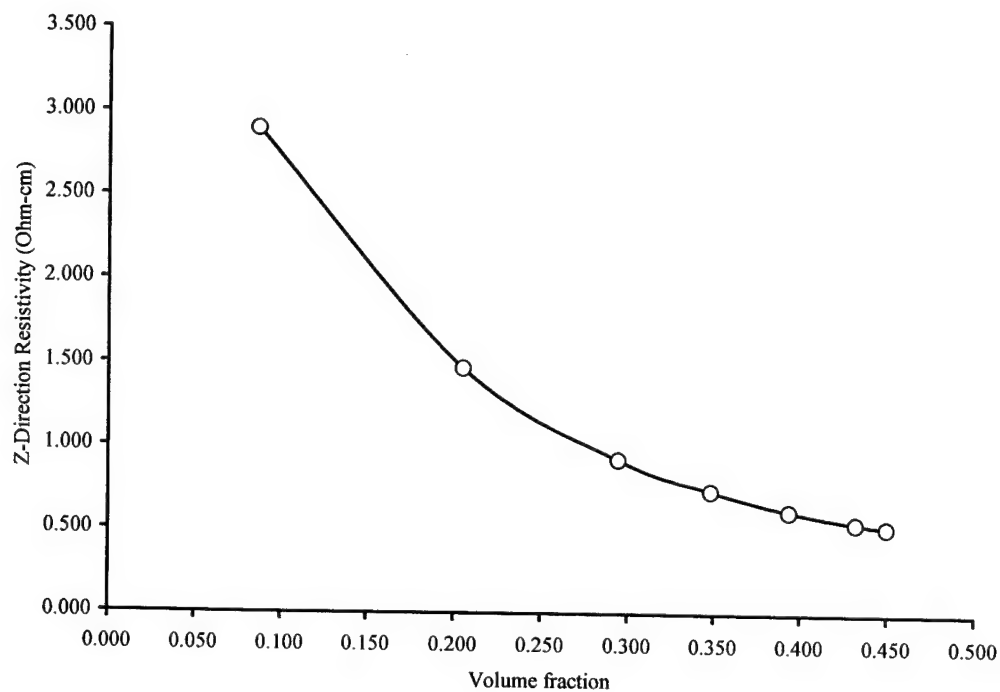
Figure 18. Z-Direction Resistivity for PR-11.
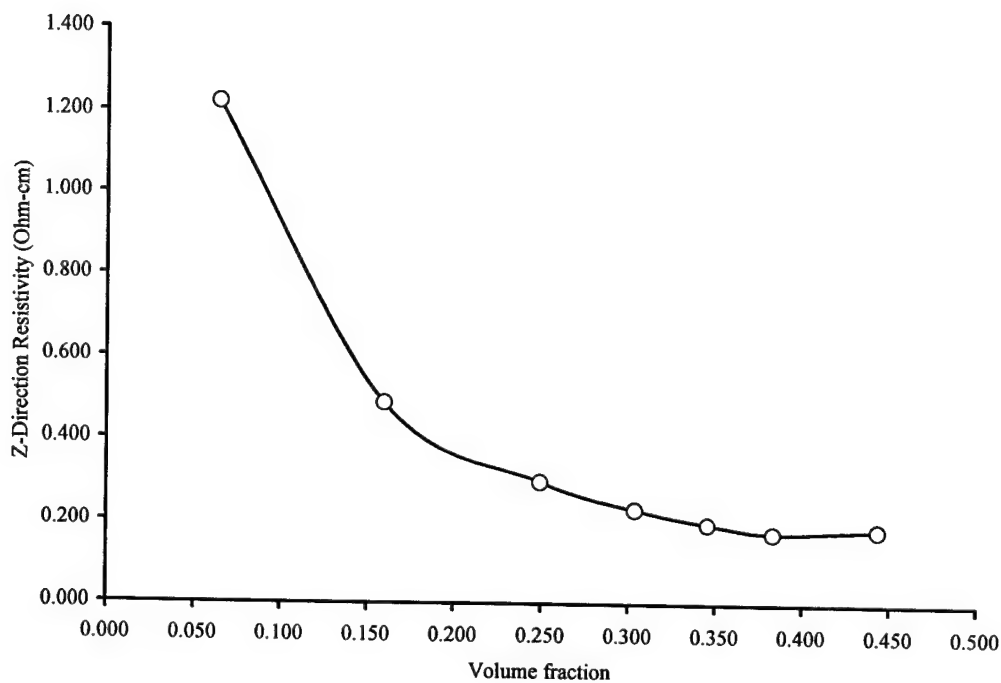
Figure 19. Z-Direction Resistivity for PR-24-PS.
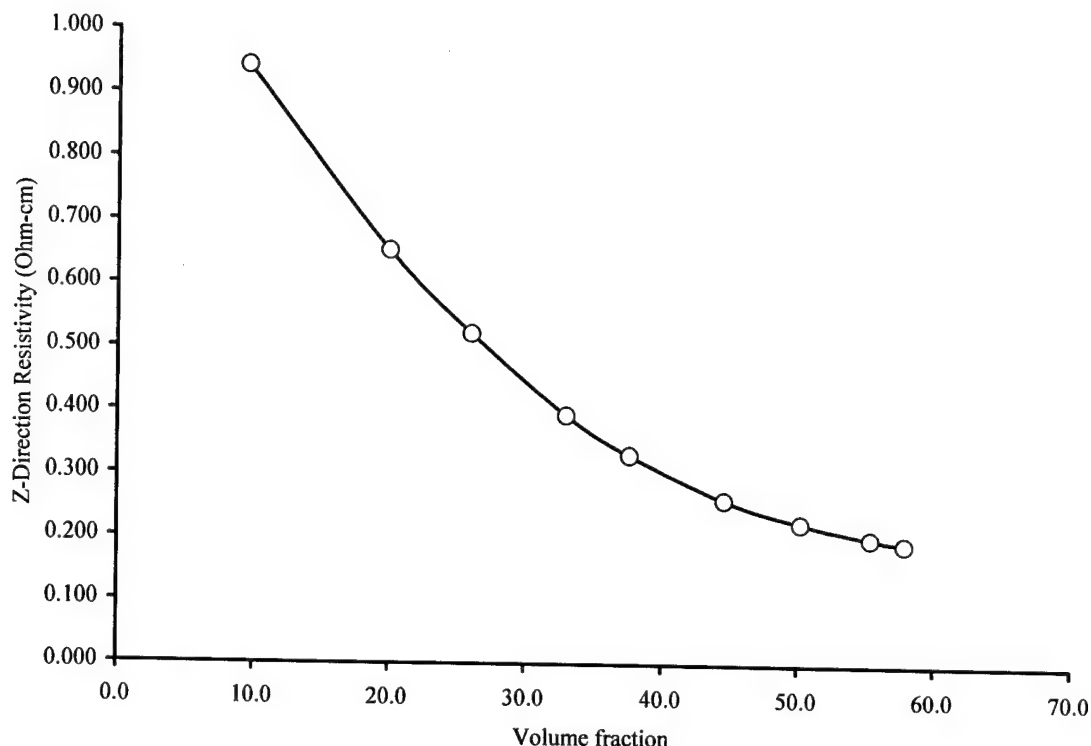
Figure 20.   Z-Direction Resistivity for an experimental nanofiber, PR-19-HT-2200, which is heat treated for maximum strength at 2200 °C instead of 3100 °C.

4.2 Coefficient of Thermal Expansion

CTE was measured in cross-linked polyester samples which had previously been manufactured but not characterized for CTE. As shown by the data below, a combination of nanofibers and chopped fiberglass proved to be more effective than nanofibers alone. Specifically, the first sample was 5% Pyrograf®-III (protocol PR-1), 10% chopped fiberglass with the balance being cross-linked polyester. The linear CTE is 25×10^{-6} °C^{-1} at 25 C, 36.2×10^{-6} °C^{-1} at 59 °C. This is very close to matching the CTE of Aluminum $(24 \times 10^{-6}$ °$C^{-1})$ and thus represents a technical success.

A second sample contained only Pyrograf®-III and CLPE (17% Pyrograf®-III by weight). In this case the CTE was is 39.5×10^{-6} °C^{-1} at 15 °C, 66.4×10^{-6} °C^{-1} at 59 °C.

Additional reinforcement might allow this material combination approach to achieve lower CTE for electronics applications; i.e., come close to matching the CTE of silicon ($\sim4.2 \times 10^{-6}$ °C^{-1}) or gallium arsenide ($\sim4.2 \times 10^{-6}$ °C^{-1}).

The measurements were made with a laser dilatometer system at University of Dayton Research Institute.
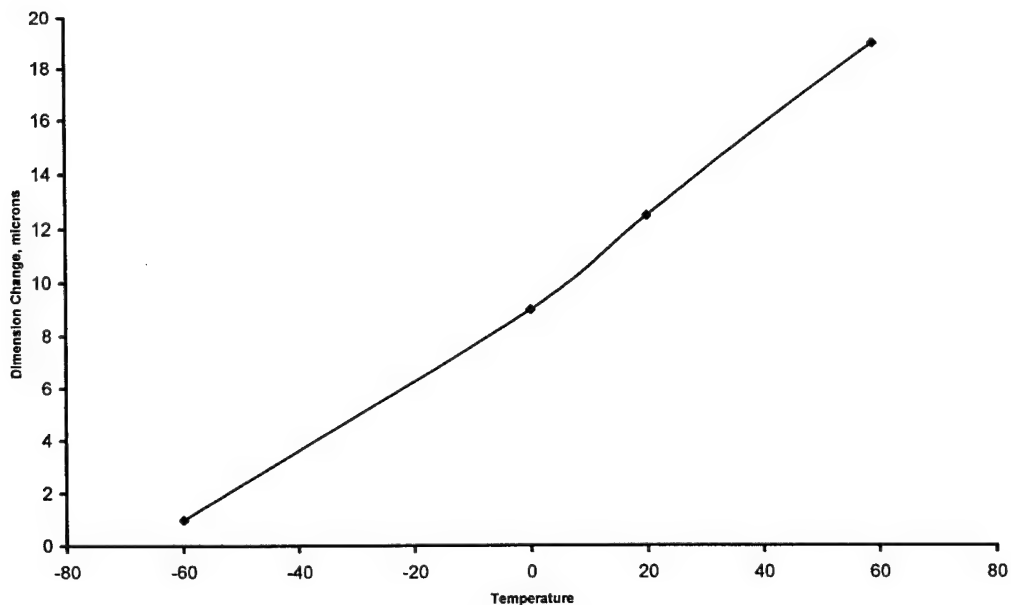
Figure 21. Thermal Expansion characteristics of Cross-Linked Polyester, 5% PR-1, 10% fiberglass. The overall CTE is 25 x 10^{-6} °C^{-1} at 25 °C, 36.2 x 10^{-6} °C^{-1} at 59 °C. This is very close to matching the CTE of Aluminum (24 x 10^{-6} °C^{-1}).

Figure 22.   Thermal Expansion characteristics of Cross-Linked Polyester, 17% PR-1, 0% fiberglass. The overall CTE is 39.5 x 10^{-6} °C^{-1} at 15 °C, 66.4 x 10^{-6} °C^{-1} at 59 °C.

TMA tests were run for each composition of carbon nanofiber in order to determine the linear coefficient of thermal expansion for Derakane samples. In general, a TMA curve

will have two linear slopes whose juncture (extrapolated) occurs at the polymer's T_g. The data obtained from TMA tests are listed in Table 3.

Table 3. TMA results for Derakane carbon nanofiber composite samples.

% Carbon Nanofiber	Trial	Coefficient of Thermal Expansion (alpha) (μm/m°C) Below Tg	Coefficient of Thermal Expansion (alpha) (μm/m°C) Above Tg
0	1	35.7	138.0
	2	37.9	125.0
	1	55.4	140.0
1.5	1	47.4	116.0
	2	41.5	137.0
1.5 (20% less silica)	1	33.4	158.0
	2	62.6	99.1
3	1	55.9	148.0
	2	40.3	125.0

The above results show a direct relationship between the linear coefficient of thermal expansion and percent carbon nanofiber present by weight. As seen in the table, a 1.5% nanofiber sample having a composition of silica that was 20 pbw less than all other composites was prepared and tested. It should be noted that for each composition of carbon nanofiber, the samples were not fully cured before the first trial. Because the TMA was run from subambient temperatures to 200 °C, the first run effectively post cured the sample while the second run yielded a result for the fully-cured composite. Therefore, observing α for the second trial of each composition analysis, there is a change in α from 37.9 to 41.5 to 40.3 μm/m°C in α below the T_g and from 125 to 137 to 125 μm/m°C above the T_g. The slope of the line used to find α below the T_g contains temperatures in the range of room temperature.

Coefficient of Thermal Expansion was also measured for NORYL® BN9003 Composites. NORYL®, made by General Electric, comes in rod and slab in several formulations. Parts are easily machined to fill a variety of needs. In addition to automotives, NORYL® is used in appliances, liquid handling equipment, and numerous other applications.

This was done partially because of the potential for automotive applications in addition to aerospace needs. Automotive manufacturers are keenly interested in inexpensive schemes to match structural aluminum.

Two types of reinforcements were used. Pyrograf®-III were trialed at 5% loading in order to compare the best types of nanofibers for this purpose. In addition, Cloisite 10 and Cloisite 25 nanoclays were used at different additive levels.

The results for Noryl show a definite effect. However the effect is not sufficient to match the CTE of structural aluminum. The development of tertiary nanocomposites combining both nanofibers and a silica or other material was not attempted for this iteration.

The nanoclays may not have not been completely exfoliated. Methods to test this include the use of XRD. Exfoliation is achieved when the individual montmorillonite platelets no longer exhibit an XRD deflection, indicating that the platelets are at least 70 angstroms apart. XRD testing was not accomplished in Phase I, although such equipment is available to us (UDRI operates an XRD system at Wright Patterson Air Force Base, which we have previously used to characterized ASI carbon fiber and carbon nanocomposites).
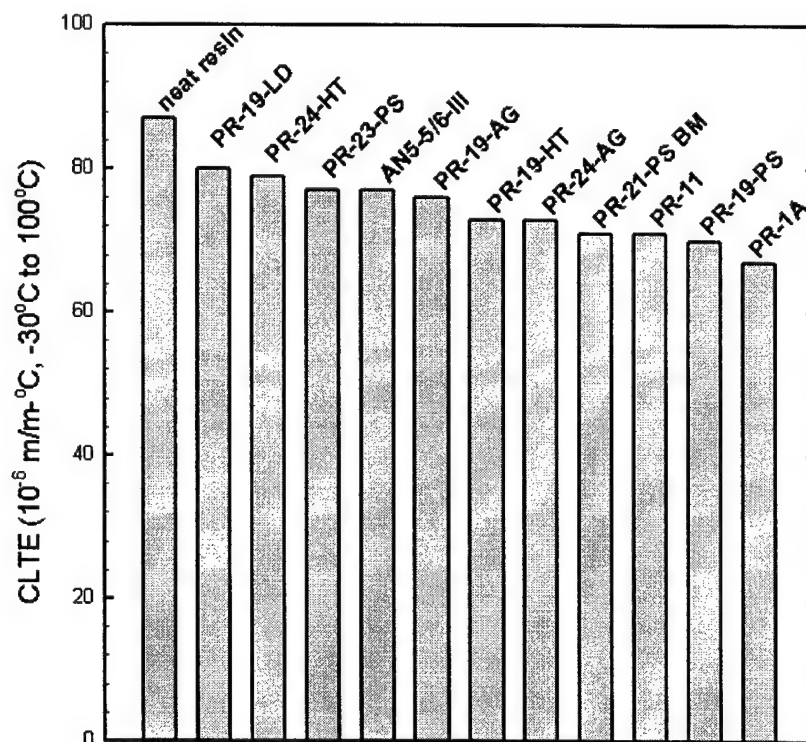
Figure 23. CTE of Noryl BN9003 Composites with 5% carbon nanofibers for various nanofiber types. These measurements were made using a mechanical dilatometer at General Motors Research.

Table 4. Composition of Noryl BN9003
composites with cloisite nanoclay reinforcements.

Sample ID	Resin	Filler	wt %	screw rev/sec	Res. Time	CTE cm/cmC	CTE Pct. Change
10A-01	BN9003	none	0%			8.84E-05	
10A-02	BN9003	Cloisite 10A	1%	100 rpm	1 min	8.46E-05	-4.32
10A-03	BN9003	Cloisite 10A	1%	200 rpm	2 min	8.48E-05	-4.18
10A-04	BN9003	Cloisite 10A	3%	200 rpm	2 min	8.38E-05	-5.24
10A-05	BN9003	Cloisite 10A	5%	200 rpm	2 min	8.12E-05	-8.20
10A-06	BN9003	Cloisite 10A	5%	200 rpm	6 min	8.22E-05	-7.05
10A-07	BN9003	Cloisite 10A	5%	100 rpm	1 min	8.40E-05	-5.06
25A-02	BN9003	Cloisite 25A	1%	100 rpm	1 min	8.70E-05	-1.61
25A-03	BN9003	Cloisite 25A	1%	200 rpm	2 min	8.54E-05	-3.46
25A-04	BN9003	Cloisite 25A	3%	200 rpm	2 min	8.42E-05	-4.78
25A-05	BN9003	Cloisite 25A	5%	200 rpm	2 min	8.20E-05	-7.26
25A-06	BN9003	Cloisite 25A	5%	200 rpm	6 min	8.14E-05	-8.02
25A-07	BN9003	Cloisite 25A	5%	100 rpm	1 min	8.32E-05	-5.95
25A-08	BN9003	Cloisite 25A	5%	100 rpm	4 min	8.38E-05	-5.23
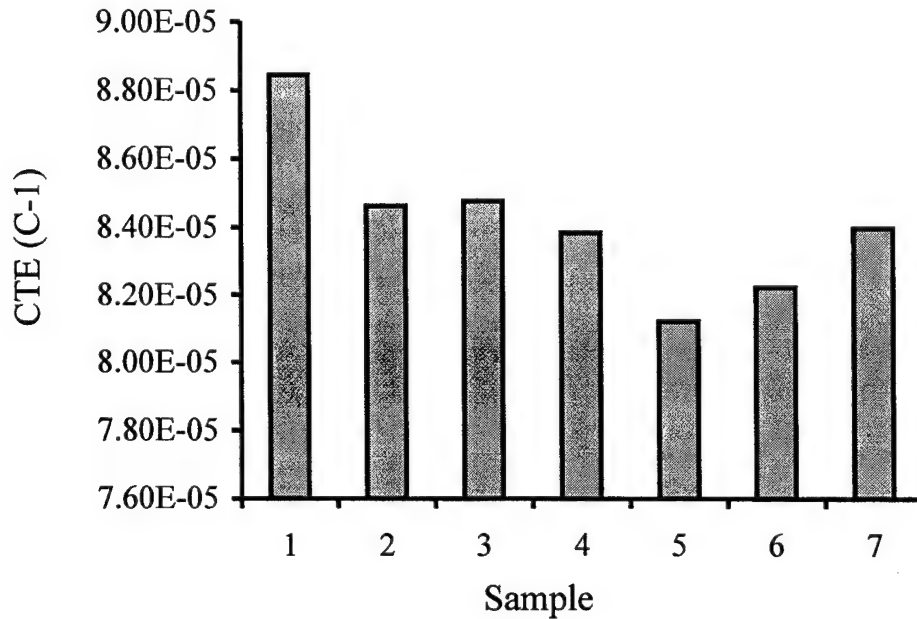
Figure 24. CTE for Cloisite 10 nanoclay reinforced BN9003 Noryl composites.
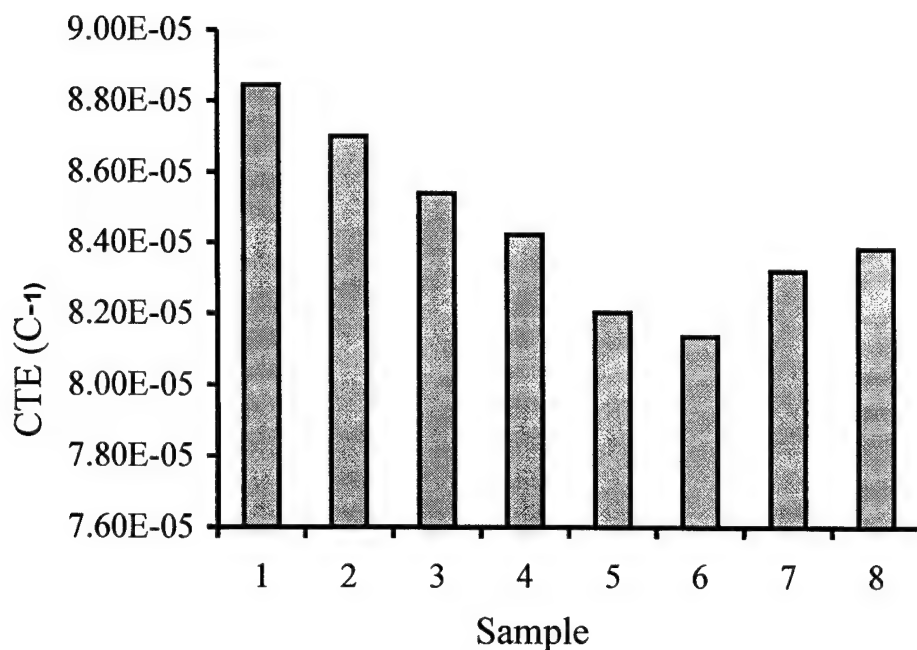
Figure 25. CTE of Cloisite 25 nanoclay reinforced BN9003 Noryl composites.

Additional samples were made using RTV silicone, Dow Corning 3145 RTV (MIL-A-46146). This material is used as a sealant for electronic fixtures and other applications, especially when environmental and corrosive applications are concerned. GE-Silicone II was also trialed, as a surrogate for spacecraft-qualified materials such as Nusil 2646 and others.

4.3 Thermogravimetric Analysis (TGA)

Thermogravimetric analysis was performed on 0%, 1.5% and 3.0% carbon nanofiber samples which had not been completely cured. As a result, an initial loss in weight was observed from residual styrene evaporating as the sample was heated. An inverse relationship was observed between the temperature at which this occurred and the weight percent carbon nanofiber present in the sample. A 0% carbon nanofiber sample had an initial loss in weight at 222.21 °C, a 1.5% sample at 206.56 °C, and a 3.0% sample at 158.87 °C. Tests were run up to 800°C from room temperature and, based on the amount of weight lost in various temperature ranges, it was concluded that acceptable mixing of silica into the copolymer matrix had taken place. As seen in Figure 28, results exhibit degradation of samples occurring at a starting temperature around 395-400 °C with complete degradation above 450 °C with little variation among samples having different compositions of carbon nanofibers. The TGA data also indicate that the silica and carbon fiber percentage in the final composites is slightly greater than the nominal amount used to fabricate the samples. This likely results from evaporation of styrene during processing.
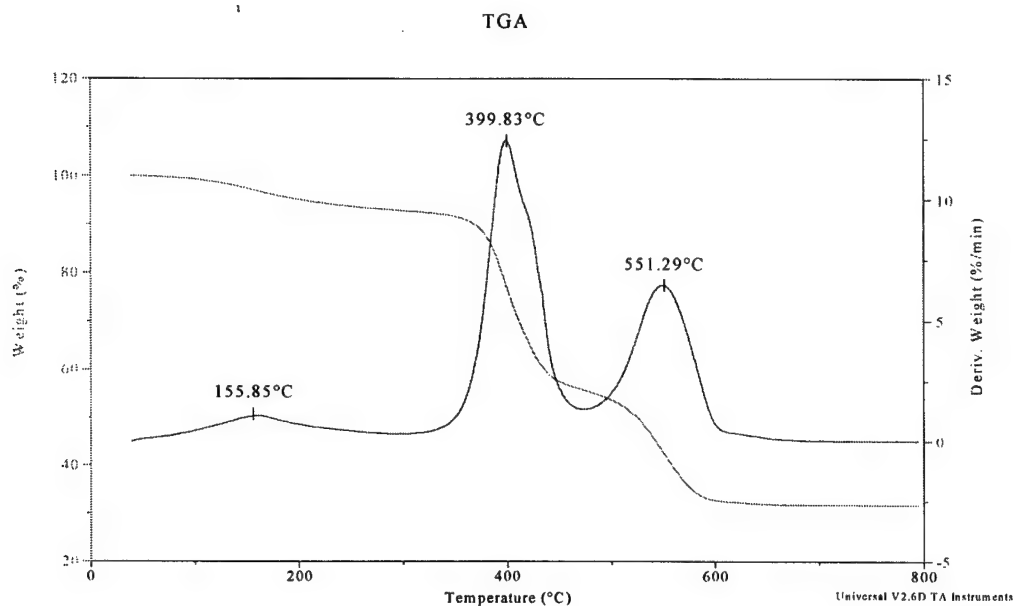
Figure 26. TGA plot of a 3% sample showing initial loss of styrene, initial material degradation around 400 °C, and complete degradation above 450 °C.

4.4 Thermal Analysis

In order to characterize the material properties of the vinyl-ester/styrene composites having variable concentrations of carbon nanofiber, a TA Instruments DSC 2910 was used for differential scanning calorimetry, a TA Instruments TMA 2940 was used for thermomechanical analysis, and a TA Instruments TGA 2950 was used for thermogravimetric analysis.

Differential Scanning Calorimetry

In performing DSC analysis of the cured, solid samples it was difficult to obtain a sample which was entirely flat and free from jagged or random geometries. In order to characterize the composites, a mixture of Derakane 470-45, silica, BPO, DMA, and carbon nanofiber was prepared using the appropriate percent composition above and mixed by hand. From this mixture, a powdered sample was removed and used for DSC analysis. The DSC result for an uncured composite containing 0% carbon nanofiber is shown in Figure 27 below. The baseline (dashed curve) shown in the figure is the DSC result for a fully-cured composite sample having 0% by weight carbon nanofiber.

32
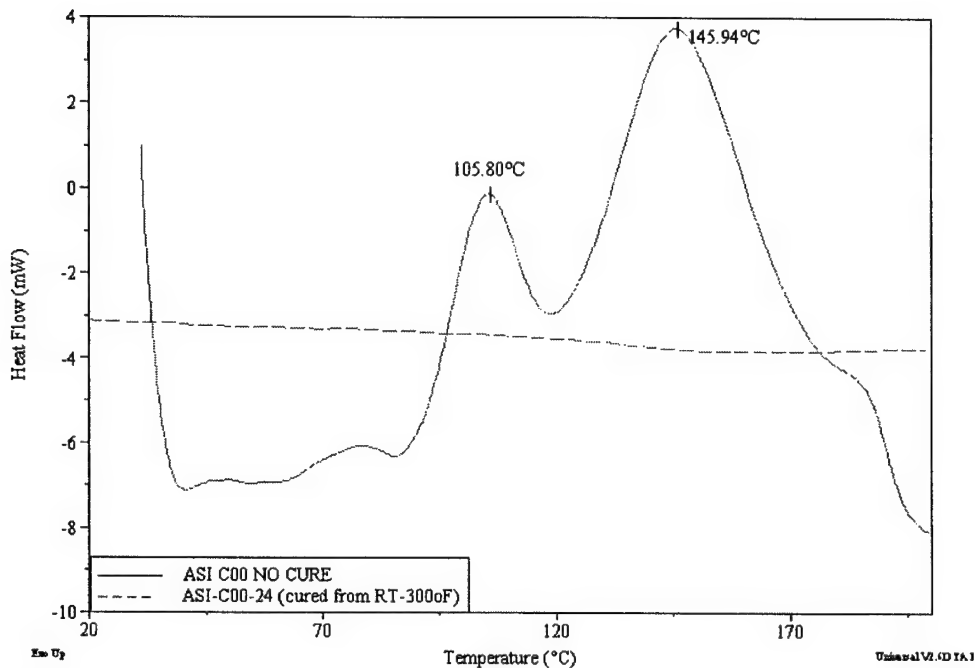
Figure 27. DSC curves for 0% carbon nanofiber composites uncured (solid) and fully cured (dashed)

Similar results were obtained for uncured 1.5% and 3.0% carbon nanofiber samples, which yielded exotherm peaks at 112°C/155°C and 110°C/152°C respectively. In Figure 27, the lower-temperature exotherm primarily results from polymerization of styrene while the higher-temperature exotherm primarily results from polymerization of the vinyl-ester monomer. Additional copolymerization reactions contribute to both exotherms.

In initial DSC characterization of the solid samples, the results were found to be inconsistent due both to sample geometry and to unreacted, residual monomer which polymerized as the sample was heated during the DSC measurement. DSC analysis of composites fabricated using the final curing process developed, in which samples were cured isobarically with a temperature ramp from room temperature to 149 °C, resulted in little or no deviation from the baseline—an indication of a high degree of cure.

4.5 Low Observables/Radar Absorbing Coatings

A BMDO funded project (DASG60-98-M-0077), demonstrated the feasibility of producing low-observable coatings that reduce reflectance in the radar band by mixing a low concentration of its Pyrograf™-III nanofibers into silicone. While this data was not developed under this program, it is directly applicable to the goals of the present effort, and so we review it here.

Coatings were made that demonstrated absorption in the range of 2-3 dB (i.e. extinction of 40-50% of incoming signal) over a broad band (2-18 GHz), and reflection loss greater than 9 dB (85-90% extinction) in a narrow band (13±0.5 GHz) when

interference effects are taken into account. These performance levels are somewhat below current state-of-the-art, which calls for 10 dB broadband reflection loss and 15 dB at interference points. However, they were achieved without benefit of studies to optimize nanofiber properties or concentration, and without application of engineering principles for design of layered/gradient structures that maximize interaction of EM radiation with the coating and tune interference phenomena. Thus there is reason for optimism that better optimization is likely to improve performance beyond the current state of the art.

Since most radar systems are tuned to work preferentially in certain narrow regions of the spectrum, it is useful to have a material that allows one to optimize interference phenomena to minimize reflectance at certain frequencies. Figure 28 shows examples of interferences that occur in the reflected signal from coatings backed by aluminum plates, which forces the transmitted signal to return along the path of the signal reflected from front surface of the coating. The two coatings that showed good overall absorption also show clear interference peaks.

This work clearly indicates that the dielectric properties of the materials can be well controlled both by the concentration and type of nanofiber included in the coating. Thus, nanofiber filled coatings can provide for a wide, continuously varied, range of dielectric coating materials that a design engineer could use to fabricate specific coating architectures that would exploit layered or gradient structures to maximize both absorption and interference effects for specific applications.
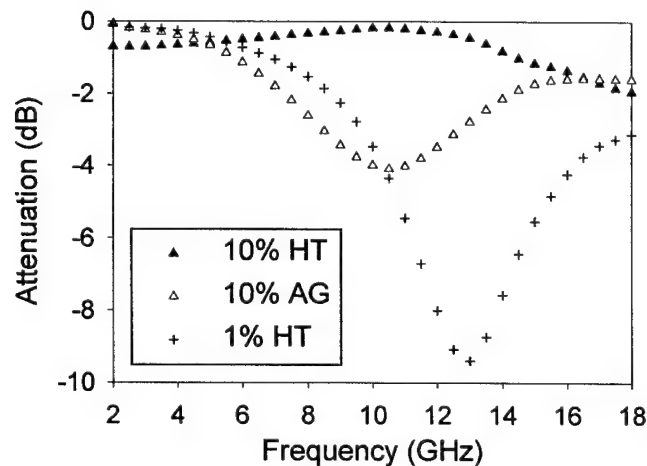
Figure 28. Interference peaks in the reflection loss from thin (~1 mm) nanofiber/silicone coatings. Data obtained at Lockheed-Martin Tactical Aircraft Systems, Ft. Worth TX.

V. APPLICATIONS

5.1. Thermoplastics Structures

A reduced-CTE thermoplastic can be used as a sunshade which would typically be used on a satellite to protect a cryogenic sensor. This is intended to benefit satellites with cryogenic sensors, as depicted below for the Next Generation Space Telescope (NGST). Although not a military mission, it has much in common with advanced reconnaissance and surveillance satellites. For example, a proposed TRW design is based on a proven technology for deploying large microwave antennae, It uses six hexagonal mirrors 3 meters between edges, which are stacked above a seventh central hexagonal mirror and are deployed and locked once the spacecraft reaches orbit. The TRW sunshade design features many shields that are deployed with masts and wires.

The sunshade umbrella must keep the telescope chilled to between -225 degrees and -180 degrees Celsius. Thermal expansion and ratcheting of these mechanisms can cause small vibrations which can limit the resolution of large-scale optics. Thus a reduced-CTE polymer nanocomposite would be a strong asset for this as well as purely military applications.
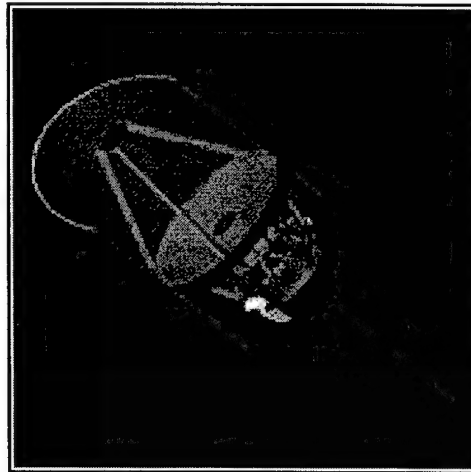
Figure 29. Next Generation Space Telescope (NGST), including sunshade, designed by TRW.

5.2 Transfer Molding of Thermoset Composites

Structural components such as fairings for launch vehicles, struts and booms for sensors as well as solar panels, can be inexpensively fabricated using transfer molding of thermoset materials such as nanofiber phenolic or nanofiber epoxy. Such materials can be much less expensive than composites manufactured by hand layup techniques.
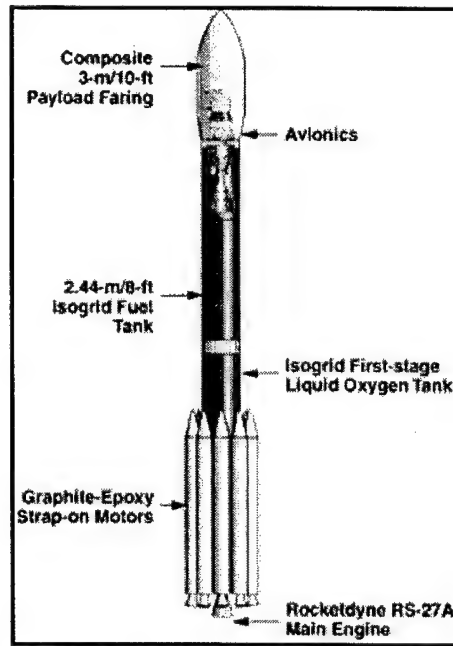
Figure 30. Transfer-molded thermosets, such as nanofiber-epoxy, would be an excellent candidate for an advanced payload fairing for launch vehicles such as the Delta pictured above, resulting in higher strength and stiffness, with less mass and less vibration damping required.

5.3. Silicone-based high thermal conductivity flexible couple

Thermal interfaces between electronic devices and thermal busses (i.e. radiators) are often technically challenging due to the discontinuity between the materials. A compliant material with a strong thermal bond would be an asset to several near-term Air Force and civilian satellite development projects.

VI. CONCLUSIONS

This effort showed that polymer nanocomposites are a realistic possibility for near-term space qualification and use on satellites. Specific observations are detailed below.

a. CTE matching to structural aluminum and titanium is achievable with several different polymer systems, such as polypropylene and cross-linked polyester. Structural applications can benefit from reduced weight and manufacturing cost, both in aerospace as well as commercial applications (such as automotives).

b. Very low CTE for enhanced structural stability during orbital sunlit/darkside transitions

36

c. Derakane compounds unexpectedly showed a variable cure rate with nanofiber addition, with a corresponding drop in performance. This family of materials requires additional investigation before it can be successfully used.

d. Electrical property enhancement was successfully demonstrated for several polymer systems. Static Charge dissipation and compliant electrical connectors are enabled.

e. Several polymer systems are compatible with reduced radar cross-section.

f. Nanocomposites can be based on already-spacecraft-qualified resins, thus reducing concerns about qualification risk.

APPENDIX A. DERAKANE 470-45 COPOLYMER PLAQUES.

Sample	Compound	Composition pbw	Composition, g	Notes
C00 - 01	Derakane 470 - 45	100	100	22.2 g Silica added before roll milling. 24.8 g Silica added on the roll mill. The mold was at RT and was then pressed for 20 seconds in a 220 F press.
	Silica	47	47	
	BPO	1.5	1.5	
	DMA	0.1	0.1	
	Pyrograf III	0	0	
C00 - 02	Derakane 470 - 45	100	50	20 - 25% of the silica added after catalysts. Good mixing observed. The mold was pre-heated in a 300 F press for 5 - 10 minutes Sample pressed for 3 - 5 minutes at 300 F.
	Silica	47	23.5	
	BPO	1.5	0.75	
	DMA	0.1	0.1	
	Pyrograf III	0	0	
C00 - 21	Derakane 470 - 45	100	50	20 - 25% of the silica added after catalysts. The mold and press were at RT. Sample pressed for 3 -5 minutes at RT
	Silica	47	23.5	
	BPO	1.5	0.75	
	DMA	0.1	0.1	
	Pyrograf III	0	0	
C00 - 22	Derakane 470 - 45	100	50	20 - 25% of the silica added after catalysts with the carbon nanofibers. The mold and press were pre-heated to 200 F for approximately 30 - 40 minutes. Sample pressed for 3 -5 minutes at 200 F.
	Silica	47	23.5	
	BPO	1.5	0.75	
	DMA	0.1	0.1	
	Pyrograf III	0.0	0.0	
C00 - 23	Derakane 470 - 45	100	50	20 - 25% of the silica added after catalysts with the carbon nanofibers. The mold and press were pre-heated to 250 F for approximately 30 - 40 minutes. Sample pressed for 3 -5 minutes at 250 F. Severe cracking observed.
	Silica	47	23.5	
	BPO	1.5	0.75	
	DMA	0.1	0.1	
	Pyrograf III	0	0	
C00 - 24	Derakane 470 - 45	100	50	20 - 25% of the silica added after catalysts with the carbon nanofibers. Pressed at RT for ~10 minutes. Heated from RT to 300 F for 50 minutes (isobaric).
	Silica	47	23.5	
	BPO	1.5	0.75	
	DMA	0.1	0.1	
	Pyrograf III	0.0	0.00	
C15 - 01	Derakane 470 - 45	100	50	12 g Silica added before roll milling. 11.5 g Silica added on roll mill. The mold and press were at RT. The mold was pressed for 20 seconds.
	Silica	47	23.5	
	BPO	1.5	0.75	
	DMA	0.1	0.1	
	Pyrograf III	1.5	0.75	

C15 - 02	Derakane 470 - 45	100	50	The mold was pre-heated in a 300 F press for 5 - 10 minutes Sample pressed for 3 - 5 minutes at 300 F.
	Silica	47	**18.5**	
	BPO	1.5	0.75	
	DMA	0.1	0.1	
	Pyrograf III	1.5	0.75	
C15 - 03	Derakane 470 - 45	100	50	20 - 25% of the silica added after catalysts with the carbon nanofibers. The mold was pre-heated in a 300 F press for 5 - 10 minutes. Sample pressed for 3 - 5 minutes at 300 F
	Silica	47	23.5	
	BPO	1.5	0.75	
	DMA	0.1	0.1	
	Pyrograf III	1.5	0.75	
C15 - 21	Derakane 470 - 45	100	50	20 - 25% of the silica added after catalysts with the carbon nanofibers. The mold and press were at RT. Sample pressed for 3 -5 minutes at RT.
	Silica	47	23.5	
	BPO	1.5	0.75	
	DMA	0.1	0.1	
	Pyrograf III	1.5	0.75	
C15 - 22	Derakane 470 - 45	100	50	20 - 25% of the silica added after catalysts with the carbon nanofibers. The mold and press were pre-heated to 200 F for approximately 30 - 40 minutes. Sample pressed for 3 -5 minutes at 200 F.
	Silica	47	23.5	
	BPO	1.5	0.75	
	DMA	0.1	0.1	
	Pyrograf III	1.5	0.75	
C15 - 23	Derakane 470 - 45	100	50	20 - 25% of the silica added after catalysts with the carbon nanofibers. The mold and press were pre-heated to 150 F for approximately 30 - 40 minutes. Sample pressed for 3 -5 minutes at 150 F
	Silica	47	23.5	
	BPO	1.5	0.75	
	DMA	0.1	0.1	
	Pyrograf III	1.5	0.75	
C15 - 24	Derakane 470 - 45	100	50	20 - 25% of the silica added after catalysts with the carbon nanofibers. Mold pre-heated at 150 F for 30-40 minutes. Pressed at 150 F for 90 minutes. Fracture present through middle, cracking.
	Silica	47	23.5	
	BPO	1.5	0.75	
	DMA	0.1	0.1	
	Pyrograf III	1.5	0.75	
C15 - 25	Derakane 470 - 45	100	60	20 - 25% of the silica added after catalysts with the carbon nanofibers Pressed at RT for ~15 minutes. Heated from RT to 300 F for 45 minutes (isobaric).
	Silica	47	28.2	
	BPO	1.5	0.9	
	DMA	0.1	0.1	
	Pyrograf III	1.5	0.90	

C30 - 01	Derakane 470 - 45	100	50	20 - 25% of the silica added after catalysts with the carbon nanofibers. The mold was pre-heated in a 300 F press for 5 - 10 minutes. Sample pressed for 3 - 5 minutes at 300 F.
	Silica	47	23.5	
	BPO	1.5	0.75	
	DMA	0.1	0.1	
	Pyrograf III	3.0	1.5	
C30 - 02	Derakane 470 - 45	100	50	20 - 25% of the silica added after catalysts with the carbon nanofibers. The mold was pre-heated in a 220 F press for 5 - 10 minutes. Sample pressed for 3 - 5 minutes at 220 F
	Silica	47	23.5	
	BPO	1.5	0.75	
	DMA	0.1	0.1	
	Pyrograf III	3	1.5	
C30 - 21	Derakane 470 - 45	100	50	20 - 25% of the silica added after catalysts with the carbon nanofibers. The mold and press were at RT. Sample pressed for 3 -5 minutes at RT
	Silica	47	23.5	
	BPO	1.5	0.75	
	DMA	0.1	0.1	
	Pyrograf III	3.0	1.5	
C30 - 22	Derakane 470 - 45	100	50	The material was in the mill for too long and became long, flaky sheets. The mold and press were pre-heated to 200 F for approximately 30 - 40 minutes. Sample pressed for 3 -5 minutes at 200 F
	Silica	47	23.5	
	BPO	1.5	0.75	
	DMA	0.1	0.1	
	Pyrograf III	3.0	1.5	
C30 - 23	Derakane 470 - 45	100	75	20 - 25% of the silica added after catalysts with the carbon nanofibers. Pressed at RT for 90 minutes at 10,000 lbs ram force. Sample exhibited upward bowing after sitting overnight.
	Silica	47	35.25	
	BPO	1.5	1.13	
	DMA	0.1	0.1	
	Pyrograf III	3.0	2.25	

REFERENCES.

1 Young-Kyun Kwon et al., "Morphology and Stability of Growing Multi-Wall Carbon Nanotubes" Phys. Rev. Lett. 79, 2065 (1997).

2 N. M. Rodriquez, J. Mater. Res. 8 (1993) 3233.

3. M. Endo, unpublished analysis.

4. E. V. Barrera, "Current Process in Nanotube Composite Characterization." *NanoSpace 2001 - The Fourth Annual International Conference on Integrated Nano/Microtechnology for Space and Biomedical Applications,* March 12th, 2001

5. Lozano, K. and E. Barrera (2001). "Nanofiber-reinforced thermoplastic composites. I. Thermoanalytical and mechanical analyses." Journal of Applied Polymer Science 79: 125-133.

6. A. Oberlin, M. Endo, and T. Koyama, J. of Crystal Growth, 32 335 (1976).

7. R. T. K. Baker, CARBON 27, No. 3, pp. 315-323, 1989

8. G. G. Tibbetts, J. Crystal Growth 66, 632 (1984).

9. N.M. Rodriquez, J. Mater. Res. 8 (1993) 3233

10. M. S. Dresselhaus, G. Dresselhaus, K. Sugihara, I. L. Spain, H. A. Goldberg, Graphite Fibers and Filaments Springer-Verlag: New York, 1988

11. C. H. Bartholomew, Catal. Rev. Sci. Eng. 24, 67 (1982)

12. R. T. K. Baker, "Chemistry and Physics of Carbon," 14 Marcel Dekker, New York, 1978

13. D. L. Trimm, Catal. Rev. Sci. Eng. 16, p. 155, 1977

14. G. G. Tibbetts, R. L. Alig, D. W. Gorkiewicz, "Production and Properties of Vapor-Grown Filaments and Fibres", International Conference on Carbon, Essen/Germany, 22-26 June (1992).

15. D. G. Glasgow et al., "Carbon Nanofiber Surface Treatment Effects on Polypropylene Composite Properties," SAMPE Advanced Materials Conference, Detroit MI, Sep 27-28, 1999, pp. 156-164.

16. H. L. Cox, Brit, J Appl. Phys. 3 (1952) 72.

17. J. Shimizu, J. Kusui, A. Tanaka, and O. Iwao, pp. 31-8 in Metal Matrix Composites: Processing, Modeling, & Mechanical Behavior, TMS (1989).

18. M. J. Hoffman, H. Liu, and G. Petzow, pp. 177-84 in Metal Matrix Composites: Processing, Modeling, & Mechanical Behavior, TMS (1989).

19. A. Srinivasan Rao and Om P. Arora, pp. 201-9 in Metal Matrix Composites: Processing, Modeling, & Mechanical Behavior, TMS (1989).

20. R. F. Gibson, *Principles of Composite Materials Mechanics*, (McGraw-Hill, NY, 1994).

21. Bohren, and D. Huffman, *Absorption and Scattering of Light by Small Particles* (Wiley, New York, 1983).

22. Pedersen, P.C. Waterman, and J.C. Pedersen, *Proc. 1985 CRDC Scientific Conf. on Obscuration and Aerosol Research*, R. H. Kohl, ed. (1985).

23. Waterman, P.C., and J.C. Pedersen, *J. Appl. Phys.*, **72**, 349 (1992).

24. Brill, R. P.; Palmese, G. R. Journal of Applied Polymer Science 2000, Vol. 76, 1572-1582 .

25. Fried, Joel R. Polymer Science and Technology; Prentice Hall, Inc.: Upper Saddle River, 1995, pp 22-48, 182-187.